A unified analysis of the in-plane and out-of-plane constraints in 3-D linear elastic fracture mechanics

A.Fernández-Canteli[1,a], E. Giner[2,b] D. Fernández-Zúñiga[1,a]

and J. Fernández-Sáez[3,c]

[1] Depart. of Construction and Manufacturing Engineering,

University of Oviedo, Campus de Viesques s/n, 33203 Gijón, Spain

[2] Centro de Investigación de Tecnología de Vehículos - CITV

Depart. de Ingeniería Mecánica y de Materiales,

Universitat Politècnica de València, Camino de Vera s/n, 46022 Valencia, Spain

[3] Depart. of Continuum Mechanics and Structural Mechanics,

University of Carlos III, Avda. Universidad 30, 28911 Leganés, Madrid, Spain

[a] afc@uniovi.es, [b] eginerm@mcm.upv.es, [c] ppfer@ing.uc3m.es

Keywords: Linear-elastic fracture mechanics, T-stress, out-of-plane constraint, thickness effect, stress intensity tensor, Williams expansion.

Abstract. A new approach is proposed, considering the tensor character of the two first terms of the generalized Williams expansion, for the analysis of the 3-D stress field near the crack front of cracked plates under mode-I loading. The attention is focused on the constraint tensor t_{ij} at the mid-plane, identified as the second order constant term of the Williams expansion, the out-of-plane component t_{33} of which seems to play a significant role in characterizing the in-plane and out-of-plane loss of the constraint. This justifies a detailed study of t_{33} using finite element analyses for through-thickness cracked plates under mode I loading with three different geometries and loading configurations: a cracked plate loaded in tension. Similar dependency with respect to thickness and crack length ratio is also observed for the in-plane component t_{11} (the so-called *T*-stress). Mutual dependencies are observed, pointing out that a unified approach to the problem is the proper way to address loss-of-constraint effects.

Introduction

The increase of the apparent fracture toughness due to the in-plane loss of constraint has been traditionally assigned to the influence of the elastic *T*-stress giving rise, both in the LEFM [1] and EPFM [2], to the so-called two-parameter approaches. Those studies are, in general, performed using specimen thicknesses greater than $B_{\min}$, what, according to the ASTM and ESIS standards, ensures plane strain conditions. This implies neglecting the presence of the often unconsidered out-of-plane t_{33} stress, as well as the variation of the t_{11} stress, i.e. the conventional *T*-stress, as a result of the specimen thickness influence. Other parameters, such as the crack depth *a/W*, typically identified with the in-plane constraint effects, may also cause a significant variation of the out-of-plane stress t_{33}.

Sustained by analytical derivations and numerical calculations, a tensor approach based on Williams expansion is proposed in [3] to define the stress and strain fields near the crack front. The study proves the independence of the structure of the stress intensity tensor k_{ij} with respect to the specimen

thickness pointing out that the increase of the apparent fracture toughness due to the loss of constraint can be only assigned to the influence of higher order terms of the stresses, in particular, of the constraint tensor t_{ij}, identified as the Williams constant term tensor, this being independent of the radial distance r. This allows us to tackle the general constraint problem under a unified approach, comprising both the in-plane and out-of-plane constraints. The consideration of the stress intensity tensor k_{ij} and the so-called constraint curves ψ_{ij} [3] (see Section 3.3) enable us to illustrate the correlation between the loss of constraint and the specimen thickness, and hence the necessity of considering the whole t_{ij} tensor, in particular, its t_{33} component.

In this work, the influence of the specimen thickness on the t_{33} and t_{11} stresses, and the relation of both to the out-of-plane strain ε_{33} are investigated. Analytical relations regarding the stress and strain tensor field at the crack front are derived, and numerical calculations are performed for determining the values of the out-of plane stress components t_{33} and t_{11}. The finite element results obtained for different configurations demonstrate the limitations of current approaches. This should contribute to a better knowledge of the in- and out-of-plane constraints as a whole, paving the way to more general new fracture criteria.

The tensor t_{ij} as a measure of constraint

Once the stress intensity tensor has been defined as:

$$k_{ij}(z;B) = k_{ij}^{*}(\theta, z;B)\Big|_{\theta=\theta_{cr}} = \lim_{r\to 0}\sqrt{2\pi r}\,\sigma_{ij}(r,\theta,z;B)\Big|_{\theta=\theta_{cr}}\,, \tag{1}$$

the condition of non-singularity of the out-of-plane strain $\varepsilon_{33}(r,\theta,z;B)$ at the crack front, along with the analytical derivations developed in [3,4] for mode-I specimens, based on the generalized Hooke's law, prove that the out-of-plane component $k_{33}(z;B)$ of the stress intensity tensor $k_{ij}(z;B)$ at the mid-plane of the specimen normal to the crack plane, satisfies the relation

$$k_{33}(z;B) = \nu(k_{11}(z;B) + k_{22}(z;B))\,. \tag{2}$$

This expression implies that $k_{33}(z;B) = 2\nu K_I(z;B)$ for any specimen thickness $0<B<\infty$, thus, verifying the necessary singularity of σ_{33} along the crack front irrespective of B, comprising the two limiting cases $B\to 0$ and $B\to\infty$. As $k_{11}(z;B) = k_{22}(z;B) = K_I(z;B)$, the stress intensity tensor becomes

$$k_{ij}(z;B) = \begin{pmatrix} K_{\mathrm{I}}(z;B) & 0 & 0 \\ 0 & K_{\mathrm{I}}(z;B) & 0 \\ 0 & 0 & 2\nu\,K_{\mathrm{I}}(z;B) \end{pmatrix}, \tag{3}$$

demonstrating the independence of the k_{ij} structure with respect to the constraint level. Contrary to what is often found in the literature, Eq. (2) does not imply plane strain conditions at the crack front since $\varepsilon_{33}\neq 0$ and ε_{33} varies along the crack front. Furthermore, because the singular terms of σ_{ij} must cancel out to impede singularity of ε_{33} at mid-plane, the following relation between the out-of-plane strain ε_{33} at the crack tip and the components of t_{ij} is found:

$$\varepsilon_{33}(z,r;B)\big|_{r=0} = \lim_{r\to 0}\frac{\sigma_{33}(r,z;B) - \nu\,(\sigma_{11}(r,z;B) + \sigma_{22}(r,z;B))}{E} = \frac{t_{33}(z;B) - \nu\,t_{11}(z;B)}{E}, \tag{4}$$

from which the corresponding tensor t_{ij} results as

$$t_{ij}(z;B) = \begin{pmatrix} t_{11}(z;B) & 0 & 0 \\ 0 & 0 & 0 \\ 0 & 0 & t_{33}(z;B) \end{pmatrix} = \begin{pmatrix} t_{11}(z;B) & 0 & 0 \\ 0 & 0 & 0 \\ 0 & 0 & E\,\varepsilon_{33}(z;B) + \nu\, t_{11}(z;B) \end{pmatrix} . \quad (5)$$

For practical values of B (notably for $B < B_{\min}$), the suitable expression for the t_{ij} tensor is given by (5) showing that the t_{33} value is in general influenced by t_{11} and ε_{33} both depending on the specimen thickness B.

Numerical calculation of the components t_{11} and t_{33} of the t_{ij} tensor

Different techniques can be applied for the calculation of the t_{ij} tensor components [5]. A direct derivation from the stress distribution, although feasible, is prone to inaccuracies in the extrapolation to the crack front. Instead, t_{11} can be determined using the interaction integral proposed by Nakamura-Parks [6]. Once t_{11} and ε_{33} are known, t_{33} can be readily obtained from (4).

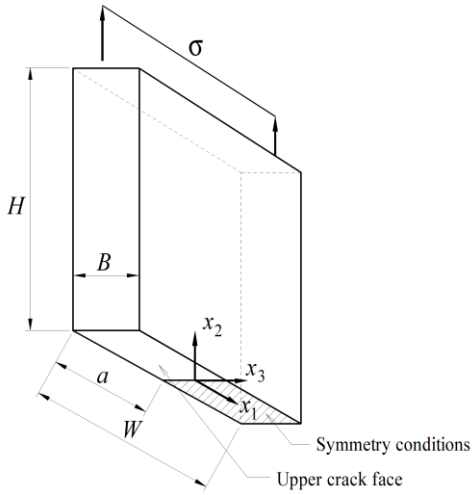

Figure 1. Geometric model of the cracked plates.

Model description. Cracked plates of different thickness B, crack depth ratios a/W and Poisson's ratios have been analysed using the FEM to check the validity of the theoretical derivations. The interest was focused on the influence of the above parameters on the t_{11} and t_{33} components of the t_{ij} tensor. Here, the analysis is restricted to plates with a straight crack front and mode-I loading. A linear elastic material with Young´s modulus $E = 207$ GPa and Poisson's ratio $\nu = 0.3$, unless otherwise stated, is considered for the numerical model as shown in Fig. 1. Fourteen different thicknesses $B = 0.1, 0.2, 0.5, 1, 2, 5, 10, 20, 35, 50, 75, 100, 200, 400$ mm and four different crack depth ratios $a/W =$ 0.1, 0.3, 0.5 and 0.7 were considered for the calculations aiming at studying the effect of thickness and crack length. A constant width $W = 50$ mm and height $H = W$ is assumed throughout the calculations, and a uniform stress $\sigma = 1$ MPa is applied on the top side of the plate in all cases. Twenty-node isoparametric elements with 3x3x3 integration points are considered. The discretization in the transverse direction comprises 50 elements.

Out-of-plane strain ε_{33}. Firstly, the out-of-plane strain ε_{33} for the different thicknesses was calculated at the mid-plane of the plate as a function of the normalized distance to the crack front in the x_1 direction, as shown in Fig. 2a. The same magnitude is depicted in Fig. 2b this time as a function of the normalized location x_3/B at the crack front. The results confirm the non-nullity of ε_{33} along the crack front in the case of plates of finite thickness. The greatest contraction is reached at a distance of about $x_1/B \approx 0.2$ ahead of the crack front.

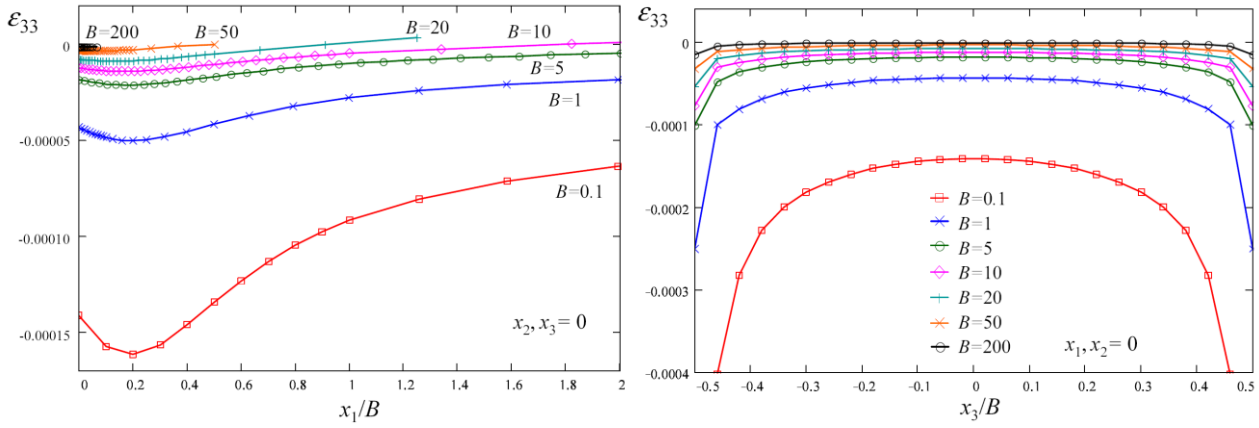

Figure 2. a) Normalized mid-plane variation of ε_{33} along the x_1-axis, and b) normalized through-thickness variation of ε_{33} along the crack front.

Constraint functions. The constraint functions $\psi_{ij}(r;B)$ represent the stress intensity fields in the direction of the prospective crack propagation ($\theta = 0$ for mode-I):

$$\psi_{ij}(r;B) = \sqrt{2\pi r}\ \sigma_{ij}(r,\theta;B)\,\big|_{\theta=0} \tag{6}$$

At the crack front, i.e. for $r \to 0$, the constraint functions ψ_{ij} converge to the respective stress intensity tensor components k_{ij} . As expected, the constraint functions converge to K_I when $r \to 0$ whereas the out-of-plane constraint function ψ_{33} converges to $k_{33} = 2\nu K_\mathrm{I}$ when $r \to 0$. This is shown in Fig. 3a, which plots ψ_{11} and ψ_{22} normalized by $k_{11} = k_{22} = K_\mathrm{I}$, and ψ_{33} normalized by $k_{33} = 2\nu K_\mathrm{I}$ at the mid-plane $x_3 = 0$ of the plate with $B = 1$ mm. Thus, the constraint functions supply relevant information about the three-dimensional stress field distribution near the crack.

For increasing r, the constrain function ψ_{33} shows a particularly noticeable decay rate, pointing out its close connection with the loss of constraint. This decay rate is strongly dependent on the specimen thickness. The constraint function ψ_{33} gets normalized with respect to B, when a dimensionless distance x_1/B to the crack front is used as abscissa (see Fig. 3b), showing the same behaviour of the decay regardless the specimen thickness. A characterization of the loss of constraint is thus possible through the simultaneous consideration of the higher tensor terms of the Williams expansion as a whole, i.e. not only through the sole consideration of the T-stress as suggested by current biparametric approaches but also considering the out-of-plane component t_{33}.

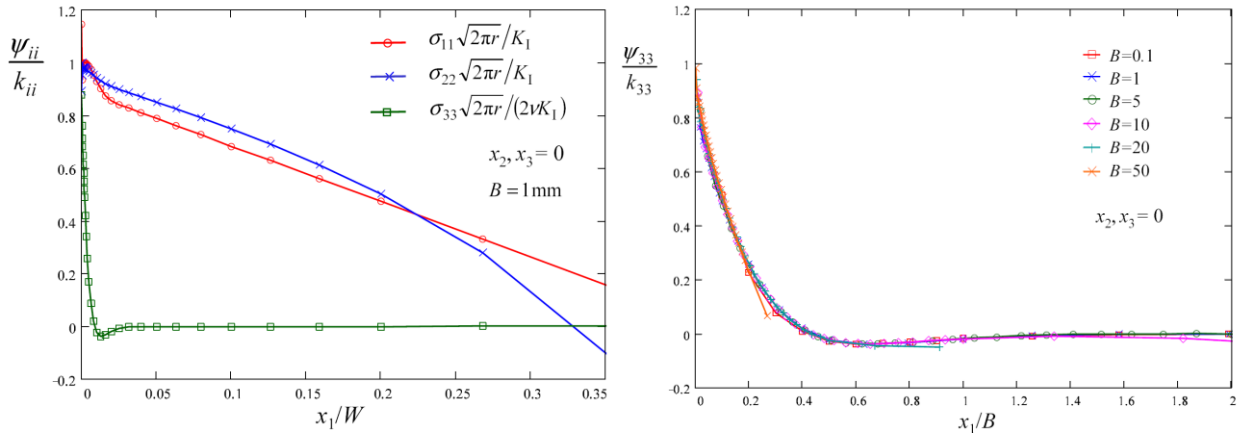

Figure 3. a) Mid-plane variation of ψ_{ii} (normalized by k_{ii}) along the x_1 axis and b) constraint curves ψ_{33} (normalized by k_{33}) for different B vs. the dimensionless distance x_1/B.

Calculation of t_{11} and t_{33}. Figures 4a) and 4b) show the results of t_{11} and t_{33} calculated at the mid-plane $x_3 = 0$ for the fourteen thicknesses B, four a/W ratios and four Poisson's coefficients. The results are normalized by an equivalent stress calculated from $K_{\text{local}}/(\pi a)^{0.5}$, where K_{local} is the mode-I SIF evaluated at that particular location of the crack front ($x_3 = 0$) using an equivalent domain integral for J. According to [4], a unique constant relationship between J and K_{local} exists, i.e. $K_{\text{local}} = (J_{\text{local}}\, E/(1-\nu^2))^{0.5}$, which is independent of the specimen thickness.

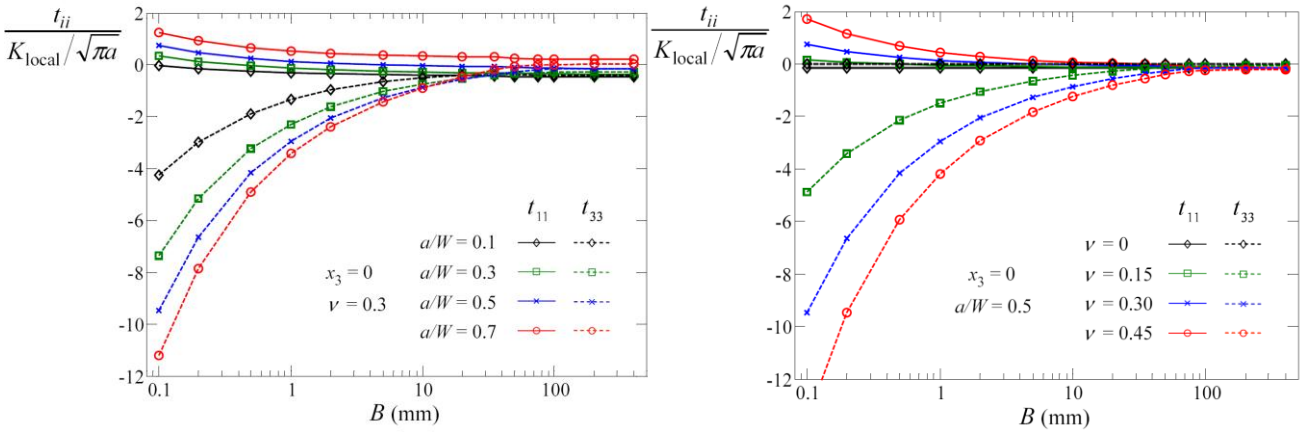

Figure 4. Variation of t_{11} and t_{33} at the mid-plane $x_3 = 0$ a) with B and a/W, and b) with B and the Poisson's coefficient ν.

Two features merit comment: Firstly, t_{33} is always negative, i.e., it is a compressive stress, whereas t_{11} can change its sign for small values of a/W tending to be negative for small a/W ratios and large B. This means that the t_{11} and t_{33} values run in opposite trend for decreasing specimen thicknesses. Secondly, the absolute magnitude of t_{33} tends to be approximately one order of magnitude greater than the magnitude of t_{11} pointing out that, in general, the effect of t_{33} cannot be neglected. Moreover, the magnitudes of t_{11} and t_{33} increase for small B, for large a/W and for large ν. As expected, the sensitivity of t_{11} to the ratio a/W is greater than to the thickness B, since t_{11} is an in-plane stress. Note that, in general, t_{11} changes with B (contrary as what is often stated in the literature) although this dependency is small for the case $a/W = 0.1$. The magnitude of t_{33} is much

more sensitive to both B and a/W being small and almost independent of a/W only for very large thicknesses.

Since all the constraint effects present in 3D crack problems are ultimately due to existence of Poisson's ratio effects, its influence is very significant [6], see Fig. 4b. Of course, for the case $\nu = 0$, there is no thickness effect and the plate behaves self-similarly throughout the thickness. Note that $t_{33} = 0$ because there is no Poisson contraction in the thickness direction. In this case, t_{11} is not zero and coincides with the value calculated for a 2D plate (the T-stress, like the SIF, is independent of ν and of the limiting 2-D case assumed, i.e. plane stress or plane strain).

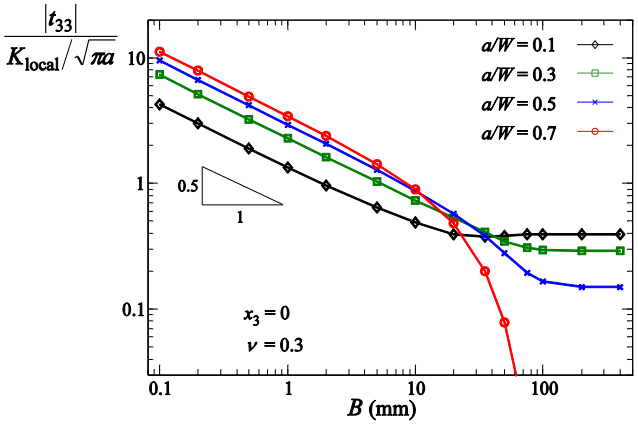

Figure 5. Log-log plot of normalized $|t_{33}|$ vs. B.

Fig. 5 shows a log-log plot of the absolute value of t_{33} (normalized by $K_{local}/ (\pi\ a)^{0.5}$) versus thickness B. It can be observed that the values fit very well to a straight line of slope −0.5 for small thicknesses (up to approximately $B = 5$ mm). Therefore, a normalization of t_{33} at the mid-plane for small thicknesses and a given a/W ratio, can be achieved using:

$$\frac{t_{33}}{K_{local}/\sqrt{\pi a}}\sqrt{B} = \text{constant}\,. \tag{7}$$

This relationship enables the approximate calculation of t_{33} for other B provided a computation for a certain B is known and the thicknesses are small. For thicknesses larger than $B = 5$ mm, the effect of the boundaries at $x_1 = \pm W/2$ increases due to the greater relative proximity of these borders and the agreement with a straight line is lost.

In Figs. 6a and 6b, the through-thickness variation of t_{11} and t_{33} for the set of fourteen thicknesses is plotted versus the normalized location x_3/B along the crack front. As for the mid-plane location analysed in previous sections, we can observe that t_{11} and t_{33} clearly increase as $B \to 0$ for all points along the crack front. In general, the magnitude at the rest of the crack front is even greater than at mid-plane. As expected, t_{11} and t_{33} converge to the 2D plane strain values as $B \to \infty$. This implies a flattening of the curves, decreasing the range of influence of the corner singularities at $x_3/B = \pm 0.5$ for large B.

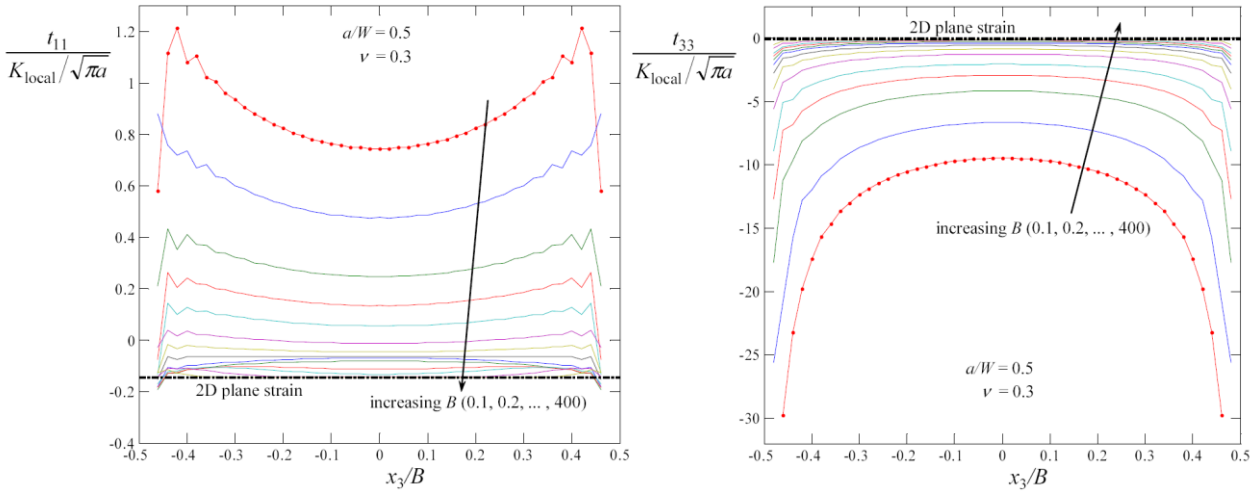

Figure 6. Through-thickness variation along the crack front for different thicknesses B, a) of t_{11} and b) of t_{33} .

Note that the value of t_{33} in the 2D plane strain problem, although small, is not zero but $t_{33} = \nu\, t_{11}$ as remarked in Section 2. The computations of t_{11} and t_{33} in the vicinity of the free surfaces must be interpreted with caution, since ε_{33} is singular at the corner intersections, and is not well calculated using finite elements. The singular behaviour of ε_{33} in these zones affects in several ways: first, the computation of the interaction integral used to calculate t_{11} tends to diverge [6]; second, the calculations of t_{11} and t_{33} through the interaction integral and Eq. (4), respectively, involve an explicit summation of ε_{33} which tends to be singular. Moreover, the validity of the extraction field used in the interaction integral (see [6]) is questioned, as the auxiliary fields corresponding to a line-load of unit magnitude assume a plane strain behaviour. Thus, the computation of t_{11} and t_{33} near the free surfaces still requires further research.

Triaxiality and constraint

Due to the lack of a satisfactory model to analyse the constraint problem in its whole complexity, some confusion has been observed in the literature referring to triaxiality and constraint. According to the analysis performed in this work, we can state that although having some similitude both definitions represents different concepts. The consideration of the constraint curves helps to understand this question. The study of the influence of the specimen thickness proves that triaxiality is ubiquitous (although with different extent): it is always present in any crack stress distribution irrespective of the specimen thickness B, both in thick specimens (when $B >> B_{min}$) as well as in thin specimens (when $B << B_{min}$) when analysed sufficiently close to the crack front. Nevertheless, these dissimilar situations clearly represent two opposite constraint states, as shown by the distinct values of the apparent fracture toughness experimentally obtained in both cases. Loss of constraint means limited triaxiality extension but by no means an “absence of triaxiality”.

Applying the constraint function concept to the analysis of the phenomenon allows us to give an adequate interpretation of the constraint role and to understand the differences and affinities of the two limiting cases $B \to 0$ (not to be mistaken with plane stress) and $B \to \infty$ (not to be mistaken with plane strain). Outside the out-of-constraint zone we can properly speak of 2-D conditions. Though the corresponding constraint curves are qualitatively similar (or even identical after being

normalized) their quantitative differences are important depending on the geometric relations. The constraint curves define the extension of the constraint zone.

Since the structure of the k_{ij} has been demonstrated to be independent of the specimen thickness, an explanation of the differences arising in the apparent fracture toughness for specimens showing different thicknesses must be found in the local fracture criterion, based on a stress fracture criterion at a certain distance of the crack front rather than in a stress intensity factor criterion, the former being influenced by the existing constraint, i.e. the t_{ij} tensor and the extension of the plastic zone.

Conclusions

The main conclusions arising from this work are the following:

- Current biparametric approaches ignore the tridimensional nature of the constant term in Williams expansion so that they cannot describe the influence of the different triaxiality degrees existing in real specimens of finite thickness. The *T*-stress alone, i.e. t_{11}, does not give information about the loss of constraint as a whole comprising both in- and out-of-plane effects.
- The validity of the biparametric approach for specimen thicknesses greater than $B_{\min}$ can be explained as a special case in which t_{33} becomes νt_{11} due to the condition $\varepsilon_{33} \approx 0$, so that t_{ij} can be expressed solely in terms of t_{11}. On the contrary, t_{ij} depends on both t_{11} and t_{33} for thinner specimens.
- The present approach proposes the use of the tensor t_{ij} , with both components t_{11} and t_{33}, for a proper definition of complex constraint states arising in real specimens. Thus, the effects of both crack length and specimen thickness on the apparent fracture toughness can be addressed.
- The constraint curves ψ_{ij} facilitate the conceptual comprehension of the loss of constraint and can be used for qualitative and quantitative assessment.
- The numerical calculations prove that specimen thickness *B* and crack depth ratio *a*/*W* exert an influence on the results of both components of the t_{ij} tensor, i.e. on t_{11} and t_{33}, the latter being more sensitive to those factors. As a result, the influence on the apparent fracture toughness cannot be merely attributed to the in-plane component.
- It is possible to normalize t_{33} for small specimen thicknesses, enabling an easy evaluation of the thickness influence on the t_{33} stress.

Acknowledgements

The authors gratefully acknowledge the financial support given by the Spanish Ministry of Science and Technology (Refs.: DPI2008-06408, BIA2010-19920 and DPI2010-20990) and by the Research Programme of the Asturian Goverment (Ref.: SV-PA-11-012).

References

[1] S. Seitl and K. Knésl: Eng. Fract. Mech. Vol. 72 (2008), p. 857
[2] C. Betegón and J. Hancock: J. Appl. Mech. Trans. of ASME, Vol. 113 (1991), p. 104
[3] A. Fernández Canteli, J. Fernández-Sáez and D. Fernández Zúñiga: Proceedings of the 12th Int. Conference on Fracture, Ottawa, July 12-17 (2009)
[4] E. Giner, D. Fernández Zúñiga, J. Fernández Sáez and A. Fernández Canteli: Int. J. Solids and Structures, Vol. 47 (2010), p. 934
[5] D. Fernández Zúñiga, J.F. Kalthoff, A. Fernández Canteli, J. Grasa and M. Doblaré: Proceedings of the ECF 15, edited by F. Nilsson (2004), Stockholm
[6] T. Nakamura and D.M. Parks: Int. J. Solids Structures, Vol. 29, (1992), p. 1597
[7] S.W. Kwon and C.T. Sun.: Int. J. Fracture, (2000) Vol. 104, p. 291
[8] M.L. Williams: J. Appl. Mech., Vol. 24, (1957) p. 109